

Supplementary Information

Monitoring technology for Cr(VI) adsorption and reduction

by operando NMR spectroscopy

Hang Zhou ^a, Xiaomeng You ^{a,b}, Xue-Lu Wang ^{a,*}, Ye-Feng Yao ^{a,*}

a. Physics Department & Shanghai Key Laboratory of Magnetic Resonance, School of Physics and Electronic Science, East China Normal University, North Zhongshan Road 3663, Shanghai 200062, P.R. China

b. Beijing Key Laboratory of Lignocellulosic Chemistry, Beijing Forestry University, Beijing 100083, PR China

**Corresponding author E-mail address:*

xlwang@phy.ecnu.edu.cn, yfyao@phy.ecnu.edu.cn

Table of Contents

1. Characterizations and Methods.....	3
1.1 Scanning electron microscopy (SEM)	3
1.2 X-ray photoelectron spectra (XPS)	3
1.3 Inductively coupled plasma optical emission spectrometer (ICP-OES)	3
1.4 Fourier Transform Infrared Spectroscopy (FTIR)	4
1.5 Ultraviolet spectrum (UV)	4
1.6 Elemental analysis (EA).....	5
1.7 Operando low-field nuclear magnetic resonance (Operando LF-NMR)	5
1.8 Liquid nuclear magnetic resonance (Liquid NMR)	6
2. Experiment	7
2.1 Materials and reagents	7
2.2 Synthesis of cellulose-based solid amine adsorbents.....	7
2.1 Equation	8
2.2 Adsorption performance test.....	10
2.3 Regeneration adsorption performance test.....	10
2.4 Computational details	10
2.5 life cycle assessment	11
3 Results and Discussion.....	13
3.1 Tables	13
3.2 Figures.....	16
4 References	29

1. Characterizations and Methods

1.1 Scanning electron microscopy (SEM)

Model: Hitachi, SU8010, Japan.

The surface morphology of the prepared adsorbents was observed with high resolution FE-SEM. The samples were dispersed uniformly into an ethanol solution and then added dropwise until the conductive gel was dry, vacuumed and then sprayed with gold. The gold was deposited with a layer of about 1 nm. The gold sprayed sample was removed and tested on the machine using a voltage of 5 kV.

1.2 X-ray photoelectron spectra (XPS)

Model: ThermoFischer, ESCALAB Xi+, USA.

This experiment was carried out using an X-ray photoelectron spectrometer. In this case, the vacuum of the analysis chamber was 8×10^{-10} Pa and the excitation source was Al ka rays ($h\nu = 1486.6\text{eV}$). The prepared adsorbent was pressed and placed flat on the test metal carrier table and attached firmly with conductive adhesive. The X-ray spot size during the test was $400\ \mu\text{m}$ and the number of scans was 20, with 50 scans for specific areas.

1.3 Inductively coupled plasma optical emission spectrometer (ICP-

OES)

Model: Agilent, 725, Germany.

Firstly, high purity Ar was used as a protective gas and after a 30min purge, the calibration solution was passed in for calibration. Then, the configured gradient standard solution was passed through. Finally, the ionic liquid of Chromium to be measured was injected into the interior of the instrument by means of a circulation pump and the concentration of the solution was calculated and analyzed.

1.4 Fourier Transform Infrared Spectroscopy (FTIR)

Model: Bruker, T27, Germany.

The KBr was dried in an oven at 150°C for 8 hours and the material to be tested was dried to a constant weight. The dried sample and KBr were ground in a mortar and pestle at a ratio of 1:100 until the KBr was in a fine powder state and then pressed into a press die under 12 Mpa pressure.

1.5 Ultraviolet spectrum (UV)

Model: Analytikjena, Specord 50 plus, Germany.

1.5 mL of a prepared solution of Cr (VI) at an initial concentration of 20 mg/L was pipetted into a glass dish, 5 mg of adsorbent was added and tested in absorption mode.

1.6 Elemental analysis (EA)

Model: Vario, EL III, Germany

The samples were weighed in disposable tin foil cups of about 1 mg and wrapped into tight, air-free regular squares before being placed in the autosampler. Before testing, three blanks were prepared and a standard sample of l-lysine was used; the test oven was brought up to 980°C by an automatic ramp-up procedure before testing.

1.7 Operando low-field nuclear magnetic resonance (Operando LF-NMR)

Model: Niumag, VTMR20-010V-1, China

(1) Operando LF-NMR

Firstly, 2 mL of aqueous $K_2Cr_2O_7$ at a concentration of $20 \text{ mg}\cdot\text{L}^{-1}$ was added to the NMR tube. Next, 5 mg of adsorbent was added. The test time was 60 min. TW: 8500; TE: 1.5; NECH 15000.

(2) Operando LF-NMR layering experiments (T_2 test for different Cr(III))

Firstly, 2 mL of aqueous $K_2Cr_2O_7$ at a concentration of $20 \text{ mg}\cdot\text{L}^{-1}$ was added to the NMR tube. Next, 5 mg of adsorbent was added. Wait for 30 min for the adsorbent to settle completely to the bottom of the NMR tube. Pulse sequence: SE-SPI; Sampling frequency: 100KHz; Number of layers: 3; Echo time: 2.0 ms.

1.8 Liquid nuclear magnetic resonance (Liquid NMR)

Model: Bruker, 500 MHz, Germany

(1) Test of end-amino hyperbranched polyamine:

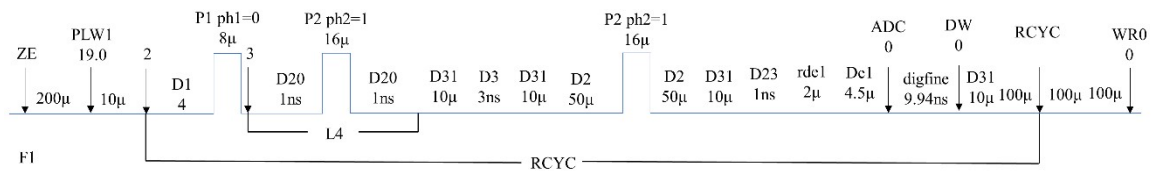
About 50 mg of end-amino hyperbranched polyamine was dissolved in 500 μl of deuterated water and the solution was shaken to mix well. The mixed reagent was then added to the NMR tube with a pulse sequence of zgdc and 4096 samples.

(2) Operando liquid NMR linewidth experiments (T_2 test for different Cr ions concentration stratification):

20 $\text{mg}\cdot\text{L}^{-1}$ $\text{K}_2\text{Cr}_2\text{O}_7$ was prepared using D_2O as solvent and 500 μL of the prepared solution was removed and 2.0 mg of adsorbent was added. After addition, the NMR tube was kept upright and the adsorbent was allowed to sink to the bottom of the NMR tube. The reference test was performed without adding any adsorbent. The cpmg1d pulse sequence was used to find the appropriate L_4 values and the gradients of L_4 values were set to 400, 1500, 2000, 3000, 4000 and 5000 as shown in Fig. S15a-d.

The operando liquid NMR test L_4 value was the best result from the above experiments, with an L_4 value of 1500. The IM-CPMG was chosen for the pulse sequence. Testing in this way allows obtaining T_2 values for different lamellar regions from the bottom to the top of the NMR tube in order to determine the Cr ion concentration in each layer region of the NMR tube.

IM-CPMG pulse sequence:



2. Experiment

2.1 Materials and reagents

Functional reagents TEPA (analytical reagent grade (AR)) and PEI (molecular weight (MW) 1,800, purity 99%), methyl acrylate (MA; AR), MCC (particle size 50 µm), epichlorohydrin (ECH; AR), and potassium dichromate ($K_2Cr_2O_7$; AR) were purchased from Shanghai Aladdin Biochemical Technology Co., Ltd. The preparation of HBP-NH₂ was conducted as previously described.^{1, 2}

2.2 Synthesis of cellulose-based solid amine adsorbents

The optimized synthesis process obtained after several trials for all three adsorbents included adding 1.00 g of MCC in a beaker with 6.0 mL of NaOH and stirring well until the MCC was fully dispersed. Then, 10.00 g of TEPA, 12.00 g of PEI, or 10.00 g of HBP-NH₂ are added to the mixture, and stirred at 0°C for 5 min. Finally, 21.00 g of ECH is added to the mixture slowly, and stirring at 0°C is continued until the material is mixed

into a homogeneous solid. The resulting solid is rinsed repeatedly with deionized water until the solution pH is neutral, and the material is filtered and dried at 80°C to a constant weight in an oven. The adsorbent materials prepared using TEPA, PEI, and HBP-NH₂ are denoted herein as MCC/TEPAA, MCC/PEIA, and MCC/HBPA, respectively. The preparation scheme and resulting products are illustrated in Fig. S4. Furthermore, the control adsorbents TEPAA, PEIA and HBPA were obtained in the same way, but without the addition of MCC in the first session.

2.1 Equation

(1) The formula for calculating the density of the amino groups (1) are as follows:

$$\rho = \frac{m \cdot W}{m \cdot M} \times 1000 \quad (1)^{3,4}$$

Where m is the sample mass by elemental analysis (g); M is the relative atomic mass (mol·g⁻¹); W is the mass ratio of the elements in elemental analysis (%).

(2) The formula for the degree of branching of an end-amino hyperbranched polyamine is

$$DB = \frac{D + T}{D + T + L} \quad (2)^{1,2}$$

where DB is the degree of branching of HBP-NH₂. D is the dendritic unit. T is the end-group unit. L is the straight chain unit.

(3) The removal rate is calculated by equation (3) as

$$q = \frac{(C_0 - C_t) \times V}{m} \times 100\% \quad (3)$$

where η (%) is the removal rate of the adsorbent material and C_0 (mg·L⁻¹) and C_t

($\text{mg}\cdot\text{L}^{-1}$) are the initial heavy metal ion concentration and the t-time heavy metal ion concentration respectively.

(4) The formula for calculating the regeneration efficiency (4) is

$$\gamma = \frac{q_n \times 100}{q_1} \quad (4)$$

where γ (%) is the regeneration rate of the adsorbent material, q_1 ($\text{mg}\cdot\text{g}^{-1}$) and q_n ($\text{mg}\cdot\text{g}^{-1}$) are the initial heavy metal ion adsorption capacity and the nth heavy metal ion adsorption capacity, respectively.

(5) The proportions of Cr(III) obtained is

$$\eta = \frac{a_0 - a_n}{a_0} \times 100\% \quad (5)$$

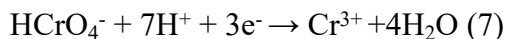
where η (%) is the proportions of Cr(III) obtained, a_0 (ms) and a_n (ms) are T_2 values at times 0 and n, respectively.

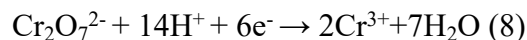
(6) The means of quantifying paramagnetic ion concentrations in solution by low-field NMR relaxometry is indicated from eqn (6)

$$\frac{1}{T_2} = \frac{12\pi^2 \gamma_p^2 \eta \mu_{eff}^2 N}{5KT} \quad (6)$$

where the transverse relaxation rate ($1/T_2$) is related to the hydrogen gyromagnetic ratio (γ_p), effective magnetic moment (μ_{eff}), viscosity (η), boltzmann constant (K), temperature (T) in Kelvin, and ion concentration (N).

(7) Cr(VI) reduction formula:





2.2 Adsorption performance test

First, 15.0 mg of adsorbent material and 6.0 mL of Cr (VI) solution were added to a 15.0 mL glass conical flask. The flask was then shaken in a shaker at 30.0 °C and 150 rpm for 60 min. After completion of the adsorption experiments, the solid samples were filtered through a 0.22 µm filter tip and dried for further characterization. In addition, the concentration of heavy metal ions in the filtrate before and after adsorption was determined using an inductively coupled plasma emission spectrometer (ICP-OES). The experiment was repeated three times and the average value was taken.

2.3 Regeneration adsorption performance test

The regeneration performance of the adsorbent material is an important indicator in practical production and a key technology for reducing economic costs. These adsorbents, which had adsorbed heavy metal ions after reaching adsorption equilibrium, was collected, washed with distilled water and dried to a constant weight. Subsequently, 15 mg of adsorbent material was shaken with 10.0 mL of NaOH solution at a concentration of 0.1 mol·L⁻¹ in a 15 mL conical flask for 60 min at 150 rpm on a shaker at 30.0°C and repeated three times. Finally, the filtrate was washed with distilled water until near neutral and dry and then reused.

2.4 Computational details

The geometries of MCC/TEPAA, MCC/PEIA and MCC/HBPA were optimized via Gaussian 09 D01^[1] at Lee–Yang–Parr gradient-corrected correlation functional (B3LYP) hybrid functional ^[2, 3] with Grimme’s DFT-D3 (BJ) empirical dispersion correction ^[4] and the def2-SVP ^[5,6] basis set level of theory, and harmonic frequencies were performed at the same level to verify that all structures correspond to the minima on the potential energy surfaces. And all above calculations have considered the water implicit solvent via SMD (Solvation model density) solvation model ^[7].

2.5 life cycle assessment

The life cycle assessment of adsorbents in this paper was based on ISO-14040 and ISO14044.⁵ The first step entails the definition of objectives and scope, the second step is the inventory analysis, the third step is the impact evaluation and the fourth step is the interpretation of the results.

The objective of this life cycle assessment was the comparative evaluation of the environmental load and water footprint of the sorbents. The scope was defined from cradle to gate (from extraction of raw materials to product preparation) and illustrated in Fig. S13. The process included the sorbent preparation process and the adsorption and reuse processes of the adsorbents. It was assumed that each adsorbent was reused five

times. In addition, the transport process of the adsorbent was ignored and was considered on the basis of ready-to-use laboratory preparation. The feedstock was used as the foreground.

It is worth emphasizing that all data were from actual data in the laboratory and the background data were taken from the databases. Background data, such as the materials and energy of three types of PLA-based bottles, were extracted from the CLCD-China-ECER0.8.1 (CLCD, 2013) and Ecoinvent-Public2.2.0 (Ecoinvent, 2008) databases in eFootprint software, which was based on ISO 14040/44 series.

For the impact evaluation, the Characterization indicators we selected include the global warming potential (GWP, kg CO₂ eq.), primary energy demand (PED, MJ), water use (WU, kg), acidification potential (AP, kg SO₂ eq.), abiotic depletion potential (ADP, kg Sb eq.), eutrophication potential (EP, kg PO₄³⁻ eq.), respiratory inorganics (RI, kg PM_{2.5} eq.), photochemical ozone formation (POFP, kg NMVOC eq.), ecotoxicity (ET, CTUe) and human toxicity-cancer effects (HT-cancer, CTUh). As the main application scenario for heavy metal adsorbent materials was water related, we focused on the water footprint (Fig.S14).

3 Results and Discussion

3.1 Tables

Table S1. Characterization indicators of MCC/TEPAA, MCC/PEIA and MCC/HBPA.

Characterization indicators	MCC/TEPAA	MCC/PEIA	MCC/HBPA
GWP (kg CO ₂ eq)	1.23E-04	8.65E-05	1.73E-04
PED (MJ)	2.40E-03	1.80E-03	3.16E-03
WU (kg)	-2.55E-01	-2.55E-01	-2.54E-01
AP (kg SO ₂ eq)	6.95E-07	5.91E-07	1.01E-06
ADP (kg antimony eq.)	1.93E-08	1.66E-08	1.95E-08
EP (kg PO ₄ ³⁻ eq.)	3.60E-07	2.33E-07	3.48E-07
RI (kg PM2.5 eq.)	1.10E-07	5.85E-08	1.98E-07
ODP (kg CFC-11 eq.)	5.59E-11	2.72E-11	5.22E-11
POFP (kg NMVOC eq.)	4.71E-07	3.48E-07	4.69E-07
ET (CTUe)	7.07E-05	3.84E-05	6.34E-05
HT-cancer (CTUh)	1.18E-12	6.57E-13	1.10E-12

Table S2. Concentrations (at%) of individual nitrogen states based on XPS N 1s peak analyses obtained for the three adsorbents after Cr(VI) adsorption.

Content (%)	N 1s					
	N-Cr	-NH ₃ ⁺	Amide	1° amine	2° amine	3° amine
MCC/TEPAA-Cr	30.11	6.57	—	26.46	26.27	10.59
MCC/PEIA-Cr	27.80	9.76	—	19.44	23.62	19.38
MCC/HBPA-Cr	23.13	4.17	3.85	26.37	23.56	18.92

Table S3. Nitrogen concentrations (at%) obtained by elemental analysis and XPS N 1s

peak analyses for the three adsorbents.

Adsorbent	N content	Amino density (mmol·g ⁻¹)	N 1s			
			Amide	1° amine	2° amine	3° amine
MCC/TEPAA	15.62%	11.16	—	29.76%	43.89%	26.35%
MCC/PEIA	15.59%	11.14	—	25.76%	39.71%	34.53%
MCC/HBPA	15.65%	11.17	8.06%	19.78%	44.78%	27.38%

Table S4. Binding energy of N 1s in MCC/TEPAA, MCC/PEIA and MCC/HBPA.

E _B (eV)	N 1s			
	amide	1° amine	2° amine	3° amine
MCC/TEPAA	-	398.80	398.15	400.80
MCC/PEIA	-	398.80	398.15	400.80
MCC/HBPA	401.08	398.80	398.15	400.80

Table S5. Binding energy of Cr 2p and N 1s in MCC/TEPAA-Cr, MCC/PEIA-Cr and MCC/HBPA-Cr.

E _B (eV)		MCC/TEPAA	MCC/PEIA	MCC/HBPA
N 1s	-NH ₃ ⁺	401.40	401.40	401.40
	Amide	-	-	401.08
	N-Cr	399.65	399.65	399.65
	Primary amine	398.80	398.80	398.80
	Secondary amine	398.15	398.15	398.15
	Tertiary amine	400.80	400.80	400.80
Cr 2p	Cr=O, Cr(VI)	587.69	577.92	587.69
	Cr-O, Cr(VI)	586.41	576.47	586.41
	Cr-N, Cr(VI)	585.13	575.46	585.13

Table S6. Gibbs free energies (*G*) associated with Cr(VI) adsorption and Cr(VI) to

Cr(III) reduction for MCC/TEPAA, MCC/PEIA, and MCC/HBPA adsorbents at 298 K

and 1 atm based on the DFT calculations illustrated in Fig. S18a–c.

Molecule	G (a.u.)	ΔG (a.u.)	Reaction
Cr (VI)	-1040.27 2	—	—
Cr (III)	-1043.71	—	—
MCC-TEPAA	- 1838.887	-3.0 07	MCC-TEPAA + Cr (VI) \rightarrow MCC-TEPAA ³⁺ + Cr (III)
MCC-TEPAA ³⁺	- 1838.456		
MCC-PEIA	-1987.56 1	-2.9 88	MCC-PEIA + Cr (VI) \rightarrow MCC-PEIA ³⁺ + Cr (III)
MCC-PEIA ³⁺	-1987.11 1		
MCC-HBPA	-1205.23 1	-2.94	MCC-HBPA + Cr (VI) \rightarrow MCC-HBPA ³⁺ + Cr (III)
MCC-HBPA ³⁺	-1204.73 3		

3.2 Figures

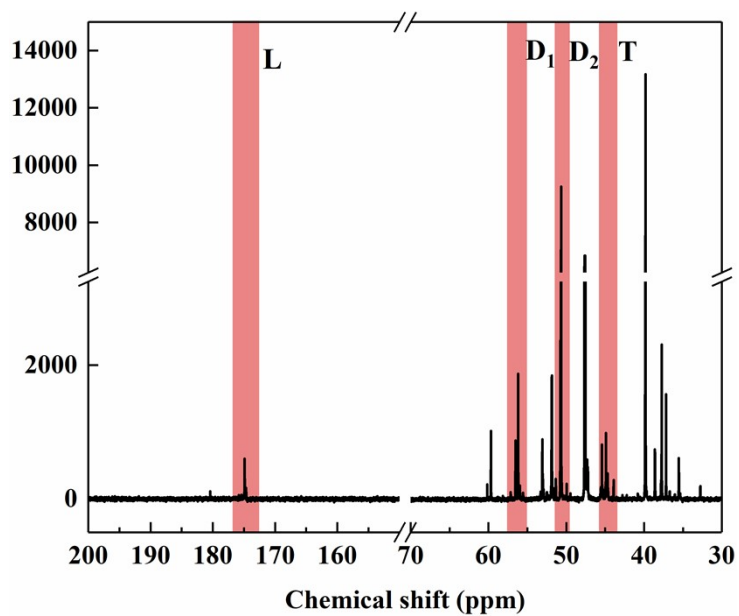


Fig. S1 ^{13}C NMR spectra of HBP-NH₂.

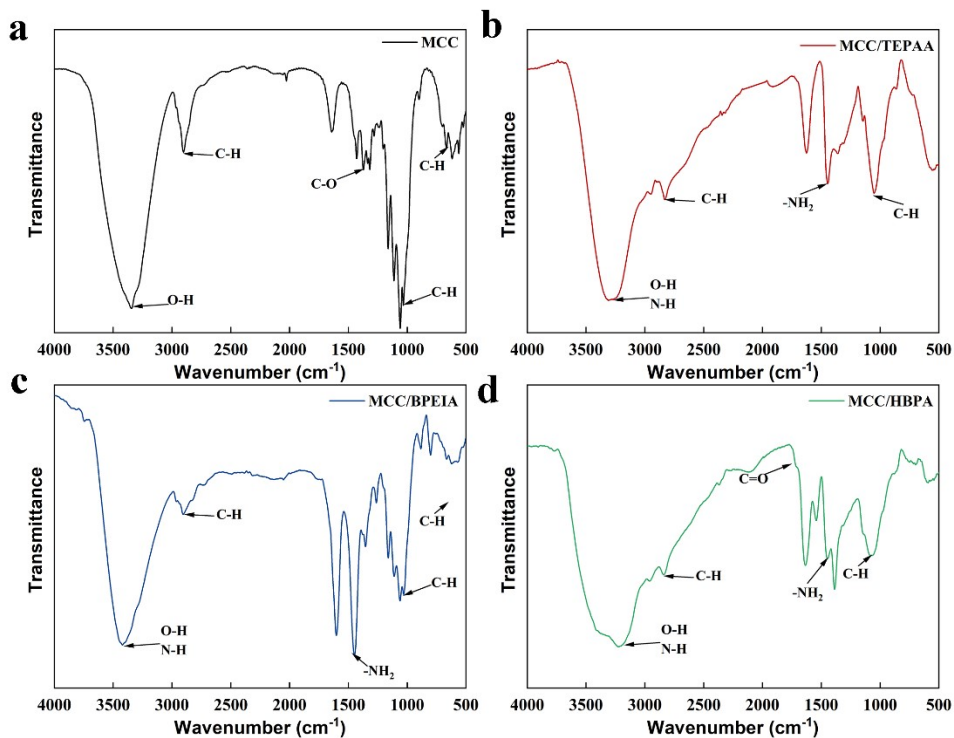


Fig. S2 FTIR spectra of MCC (a), MCC/TEPAA (b), MCC/PEIA (c) and MCC/HBPA

(d).

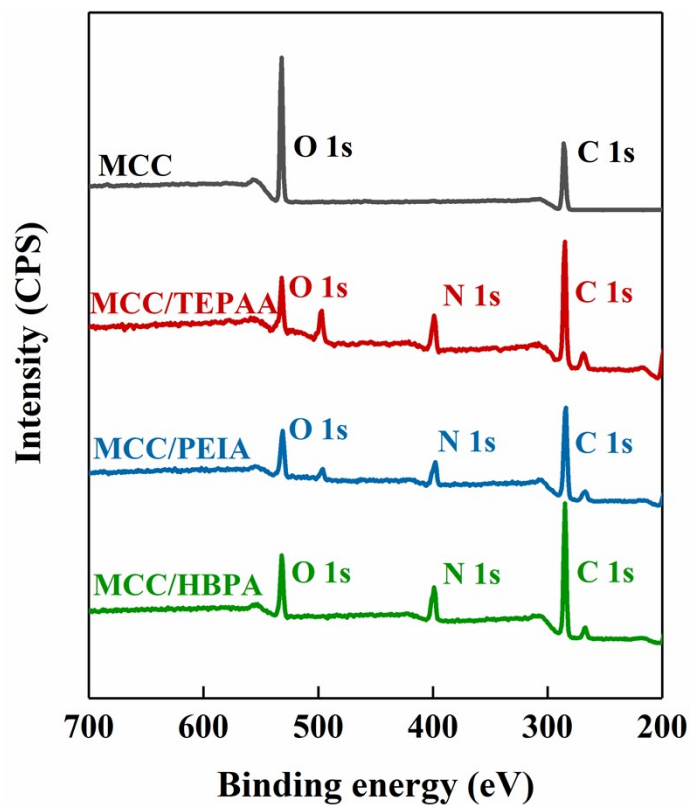


Fig. S3 wide-scan XPS spectra of MCC, MCC/TEPAA, MCC/PEIA and MCC/HBPA.

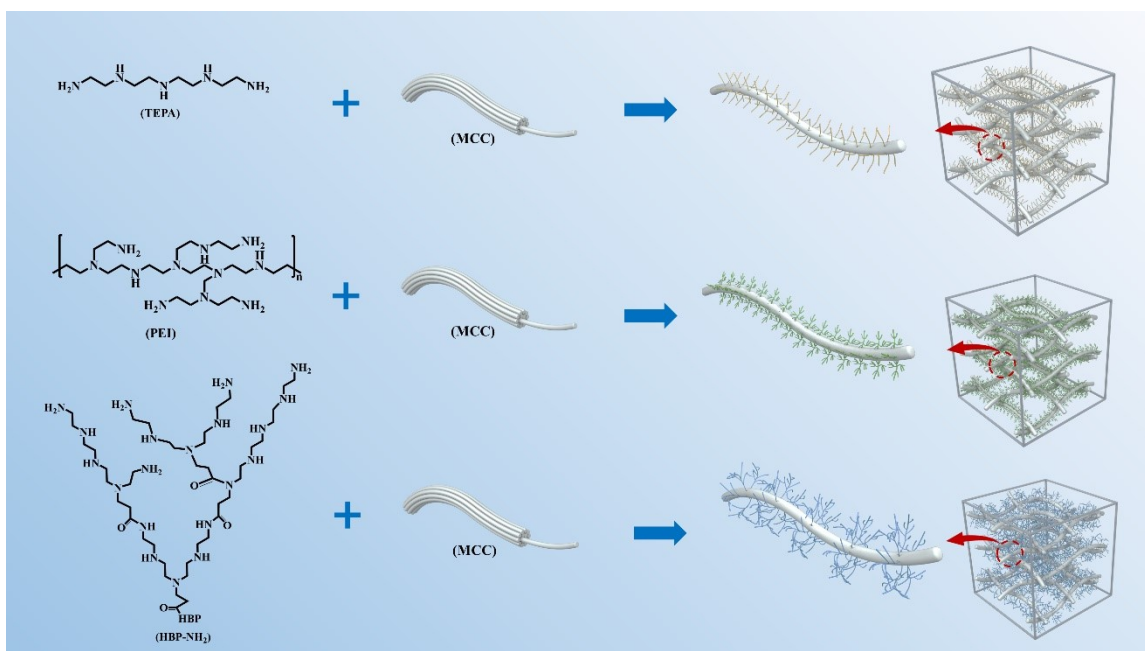


Fig. S4 Synthesis and structures of MCC/TEPAA, MCC/PEIA, and MCC/HBPA adsorbents.

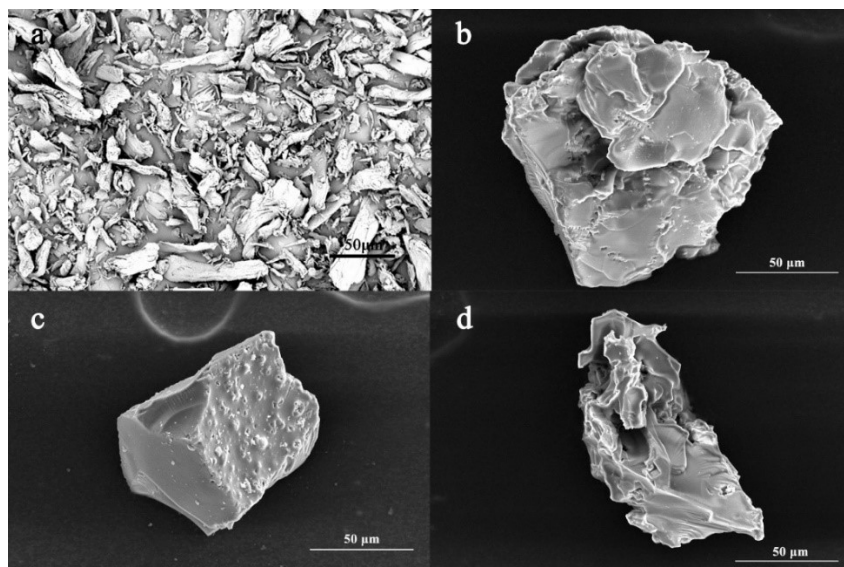


Fig. S5 SEM of MCC(a), MCC/TEPAA(b), MCC/PEIA(c) and MCC/HBPA (d).

An analysis of SEM images obtained for the MCC/TEPAA, MCC/PEIA, and MCC/HBPA adsorbents (Fig. S5 b–d) indicates that the three adsorbents exhibit a blocky morphology, and the fibrous morphology of the MCC (Fig. S5a) components can scarcely be observed in the figures, which may be due to the MCC fibers being encapsulated by the functional reagents.

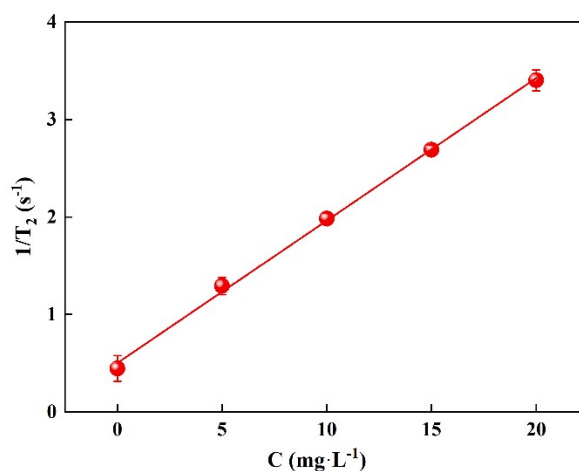


Fig. S6 Standard curve for the conversion of Cr(VI) to Cr(III)

$$(y=0.50+0.15x; R^2=0.99929).$$

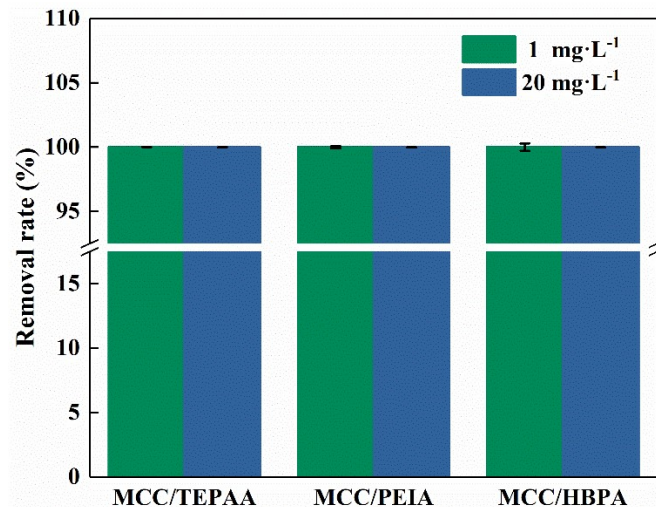


Fig. S7 Cr(VI) removal rate for two different initial Cr(VI) concentrations.

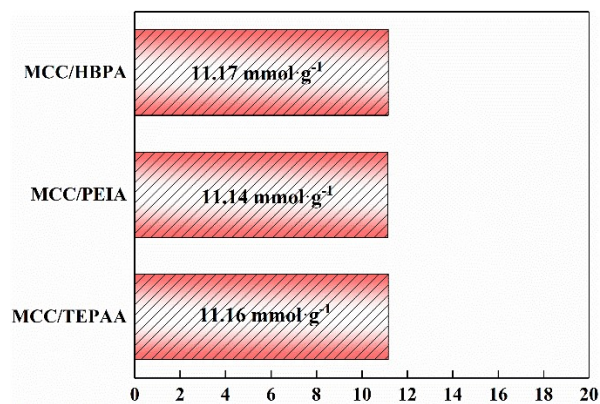


Fig.S8 The density of the functional groups and schematic diagram of structure of the three adsorbents.

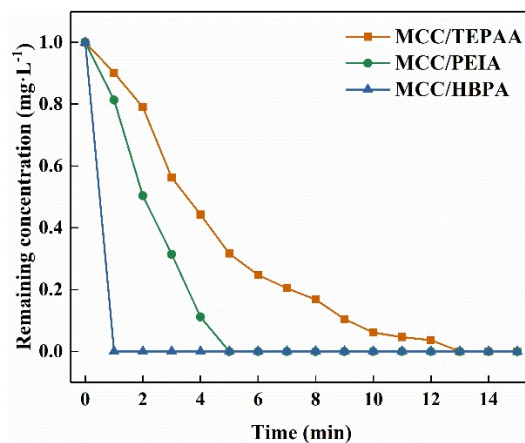


Fig. S9 Remaining Cr(VI) concentrations obtained by the three adsorbents for the low

initial Cr(VI) concentration ($1 \text{ mg}\cdot\text{L}^{-1}$) as a function of time.

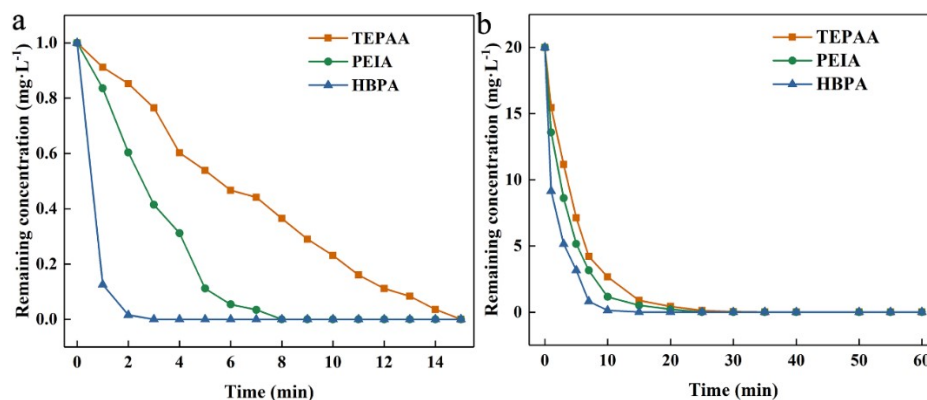


Fig. S10 Remaining Cr(VI) concentrations obtained by the three adsorbents for the low initial Cr(VI) concentration ($1 \text{ mg}\cdot\text{L}^{-1}$) (a) and high Cr(VI) concentration ($20 \text{ mg}\cdot\text{L}^{-1}$) (b)

as a function of time.

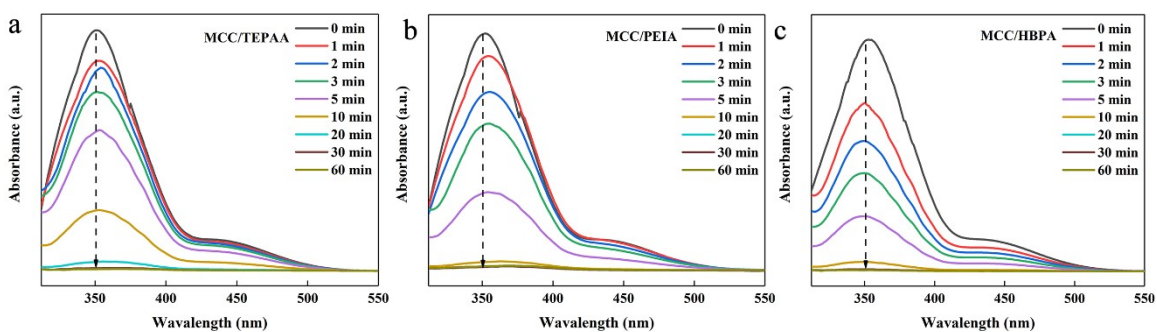


Fig. S11 a-c. UV absorption spectra indicative of Cr(VI) concentrations obtained for the three adsorbents: (a) MCC/TEPAA; (b) MCC/PEIA; (c) MCC/HBPA.

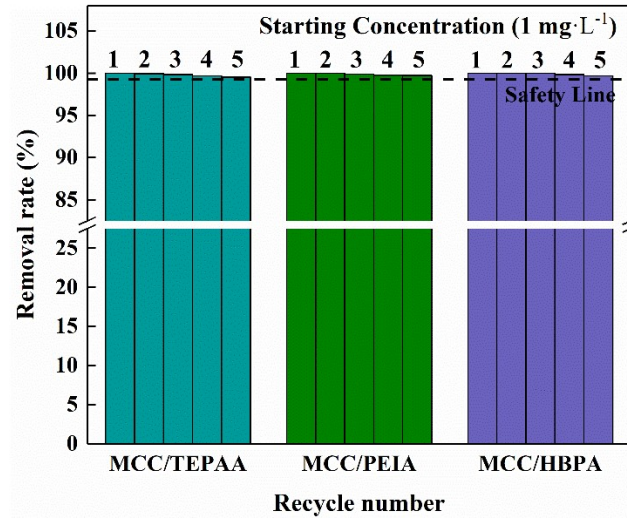


Fig. S12 Regeneration performance for the low initial Cr(VI) concentration ($1 \text{ mg}\cdot\text{L}^{-1}$).

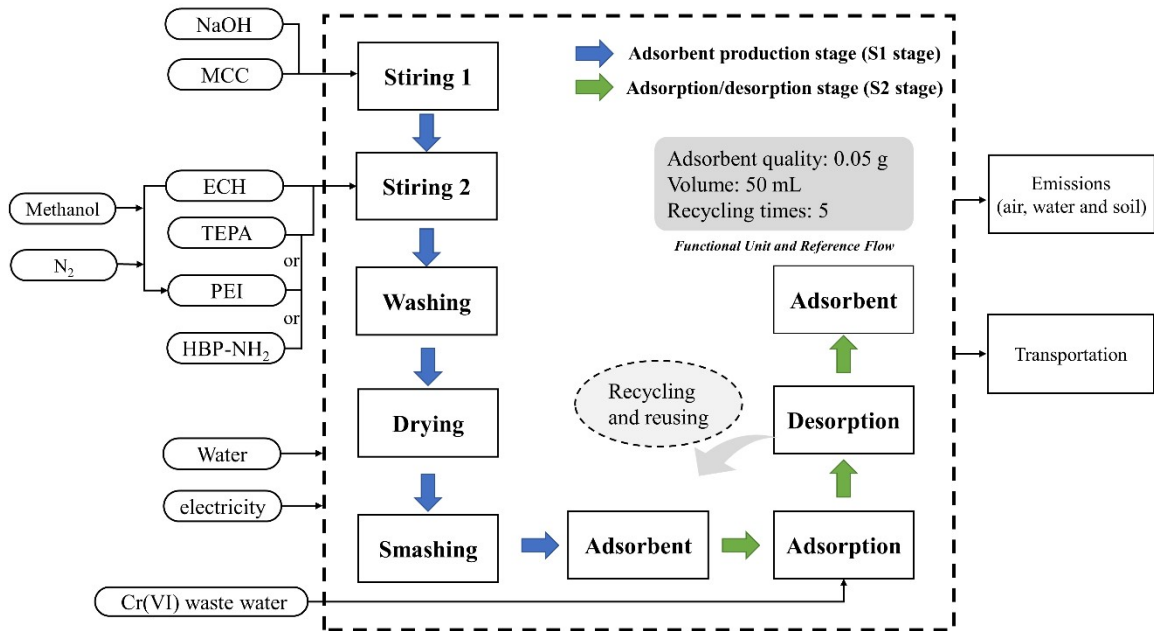


Fig. S13 Boundaries of the studied system.

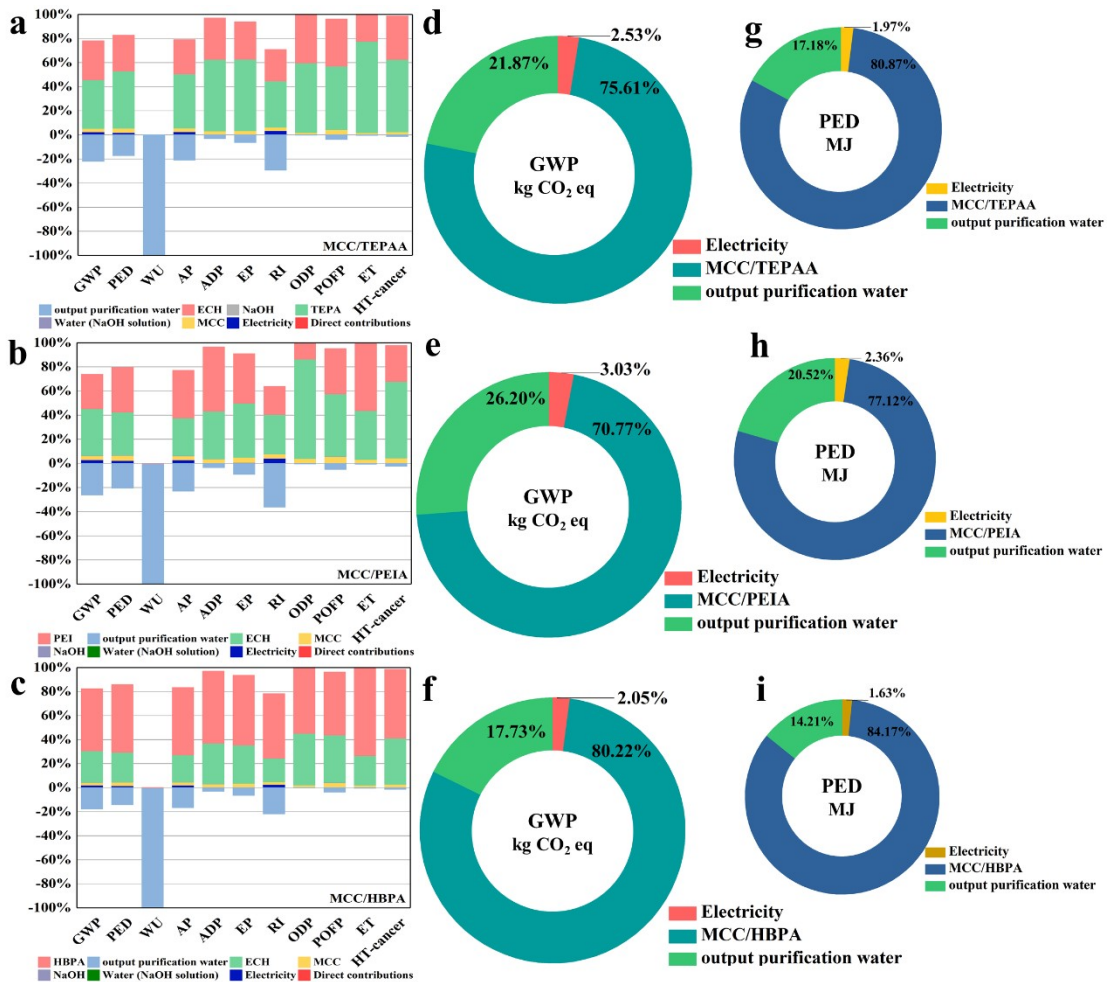


Fig. S14 Life cycle assessments of the three adsorbents based on environmental impact indicators: (a) MCC/TEPAA; (b) MCC/PEIA; (c) MCC/HBPA. Contributions to the global warming demand (GWD): (d) MCC/TEPAA; (e) MCC/PEIA; (f) MCC/HBPA. Contributions to the primary energy demand (PED): (g) MCC/TEPAA; (h) MCC/PEIA; (i) MCC/HBPA.

The life cycle assessments in this study were based on the preparation and application processes of the adsorbents, as illustrated schematically in Fig. S13. The environmental hazards associated with these processes were evaluated using various indicators, such as

global warming potential (GWP; kg CO₂ eq.), primary energy demand (PED; MJ), water use (WU; kg), acidification potential (AP; kg SO₂ eq.), abiotic depletion potential (ADP; kg Sb eq.), eutrophication potential (EP; kg PO₄³⁻ eq.), respiratory inorganics (RI; kg PM_{2.5} eq.), photochemical ozone formation potential (POFP; kg NMVOC eq.), ecotoxicity (ET; CTUe), and human toxicity-cancer effects (HT-cancer; CTUh). The values for these indicators, obtained for the three adsorbents, are listed in the Supporting Information (Table S4). The contributions of these indicators from purified water, ECH, NaOH, aqueous NaOH solution, MCC, electricity used in the processes, direct contributions, and the TEPA, PEI, and HBPA functional materials associated with the MCC/TEPAA, MCC/PEIA, and MCC/HBPA adsorbents, respectively, are presented graphically in Fig. S14a–c.

The results indicate that TEPA, PEI, HBPA, and ECH contribute the most to the environmental load across all the considered indicators. However, the adsorbents also demonstrated significant environmental benefits by generating a substantial amount of clean water. Among these indicators, the global warming potential (GWP) and primary energy demand (PED) values associated with the adsorbent preparation processes are the key contributors to environmental pollution. Therefore, the proportions of the GWP attributable to the output purified water, electricity, and the synthesis of the MCC/TEPAA, MCC/PEIA, and MCC/HBPA adsorbents are compared in Figs. S14d–f, respectively, while these attributions are provided in Figs. S14g–i for the PED value.

These results show that the synthesis of MCC/PEIA contributed less to both GWP and PED than the processes associated with MCC/TEPAA and MCC/HBPA. This is due to the low-carbon and low-energy process used in the synthesis of PEI. In contrast, the synthesis of MCC/HBPA contributed the most to both GWP and PED, as the process for preparing end-amino hyperbranched polyamines is the most complex, requiring the most energy and resulting in the highest CO₂ emissions. Overall, the life cycle assessments indicate that all three adsorbents make a positive environmental contribution by generating a significant amount of clean water.

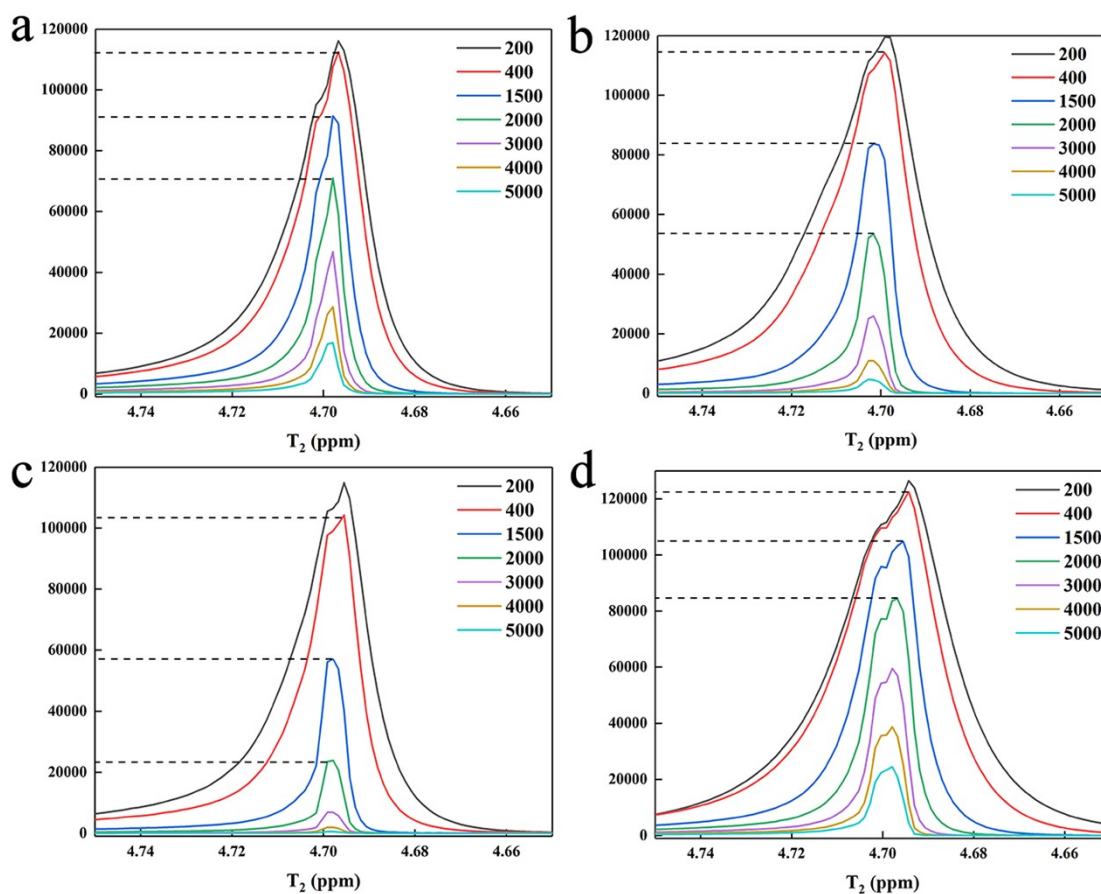


Fig. S15 a-d. Liquid NMR results of cpmg1d pulse sequences with different L_4 values

(a. no adsorbent added; b. MCC/TEPAA; c. MCC/PEIA; d. MCC/HBPA).

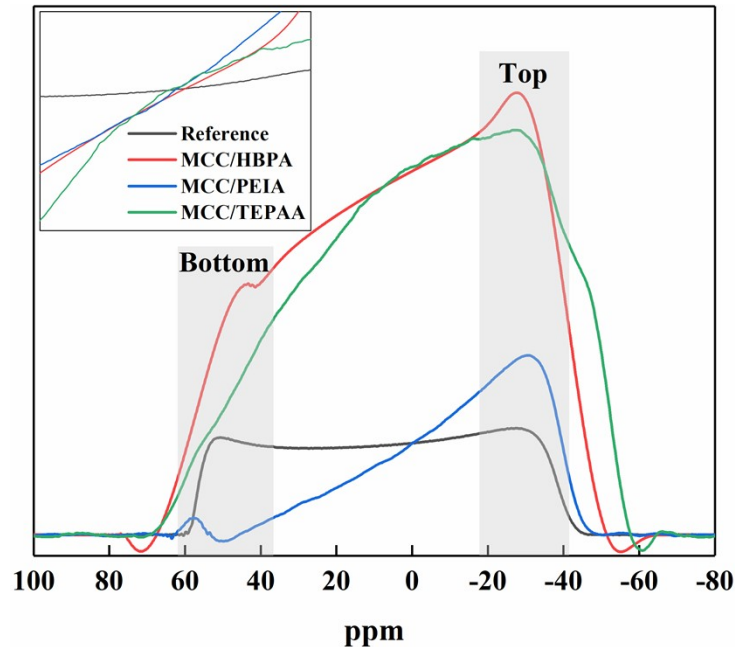


Fig. S16 Operando liquid-NMR layering experiments: Lateral relaxation time (T_2) of the im-cpmg pulse sequence and the slope in the plots running from the bottom to the top of the NMR tube.

Applying the most appropriate L_4 value of 1500 derived from preliminary investigations using a Carr-Purcell-Meiboom-Gill (CPMG) 1d sequence yielded the stratification results shown in Fig. S16. These results present clear differences between the Cr(VI) and Cr(III) concentrations in the liquid at the bottom of the NMR tube, where the adsorbent is concentrated, and at the top of the NMR tube, where the adsorbent is absent, for all three adsorbents when conducting liquid-NMR spectroscopy analyses under the IM-CPMG sequence.

The Cr adsorption rates of the adsorbents can be explicitly correlated with the slope in

the plots running from the bottom to the top of the NMR tube as shown in Fig. S8. Accordingly, these results indicate that the slope associated with the MCC/TEPAA adsorbent was the largest, followed by that of the MCC/PEIA adsorbent, and, finally, that associated with the MCC/HBPA adsorbent, which was the smallest. These findings support the full text discussion, where the Cr reduction rates of adsorbents increase with functional building blocks conforming to the order of hyperbranched structures, linear structures, and small molecules. The small molecule's structure has the best effect.

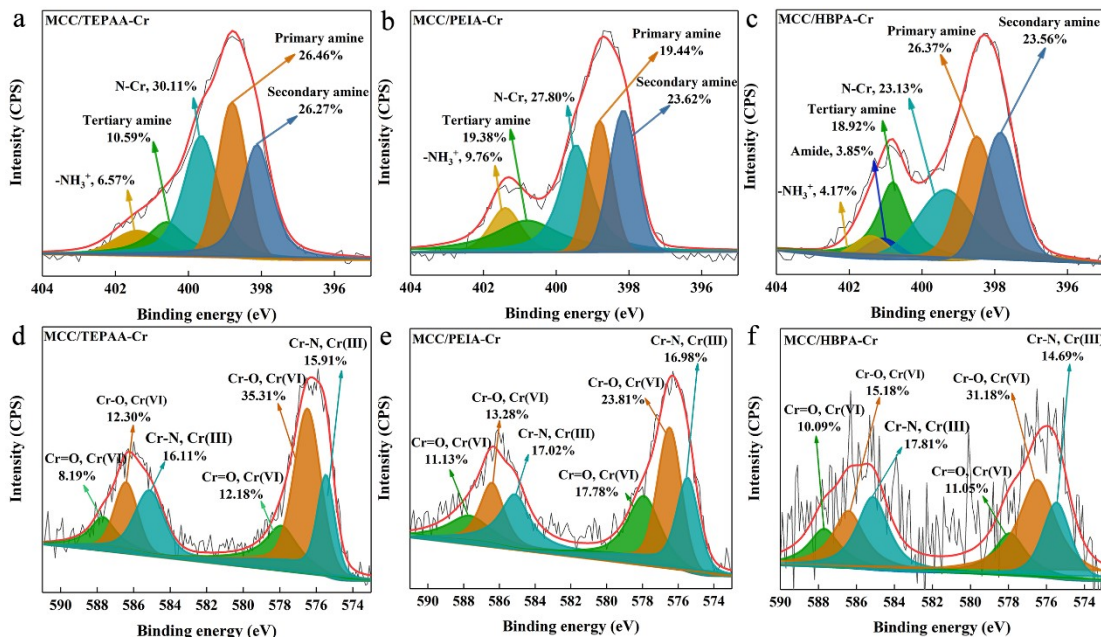


Fig. 17 Deconvoluted XPS spectra of the three adsorbents after Cr(VI) adsorption for N

1s: (a) MCC/TEPAA-Cr; (b) MCC/PEIA-Cr; (c) MCC/HBPA-Cr; and Cr 2p: (d)

MCC/TEPAA-Cr; (e) MCC/PEIA-Cr; (f) MCC/HBPA-Cr.

The interactions prevailing between Cr(VI) atoms and the adsorbents were identified by analyzing the deconvoluted XPS N 1s and Cr 2p spectra of MCC/TEPAA, MCC/PEIA,

and MCC/HBPA after Cr (VI) adsorption, which are denoted herein as MCC/TEPAA-Cr, MCC/PEIA-Cr, and MCC/HBPA-Cr, and the XPS N 1s analyses are presented in Fig. S17a–c, while the Cr 2p spectra analyses are presented in Fig. S17d–f, respectively. We note from the N 1s spectra that two new peaks appeared at binding energies of 401.40 eV and 399.65 eV, which were attributed to -NH_3^+ and N-Cr states, respectively.^{2, 4, 6} The XPS Cr 2p spectra were deconvolved into peaks with binding energies of 587.69 eV, 586.41 eV, 585.13 eV, 577.92 eV, 576.47 eV, and 576.46 eV, which were attributed to Cr(VI)=O, Cr(VI)–O, N-Cr(III), Cr(VI)=O, Cr(VI)–O, and N–Cr(III) states, respectively.⁷⁻⁹ The concentrations (at%) of the individual nitrogen states obtained for the MCC/TEPAA-Cr, MCC/PEIA-Cr, and MCC/HBPA-Cr adsorbents are listed in Table S2, where we note that the concentrations associated with the primary, secondary, and tertiary amine and amide states are all reduced relative to their corresponding concentrations prior to Cr(VI) adsorption (Table 3). Summations of the relative areas under the deconvolved XPS Cr 2p peaks associated with Cr(III) species on the MCC/TEPAA, MCC/PEIA, and MCC/HBPA adsorbents provided Cr(III) concentrations of 32.02 at%, 34.00 at%, and 35.75 at%, respectively. This is due to the fact that the total amount of reduction is related to the density of amino functional groups and the utilization rate of the density of functional groups. We note that these results are not significantly different from the results obtained via operando LF-NMR spectroscopy discussed above (i.e., 24.84%, 26.15%, and 27.58%).

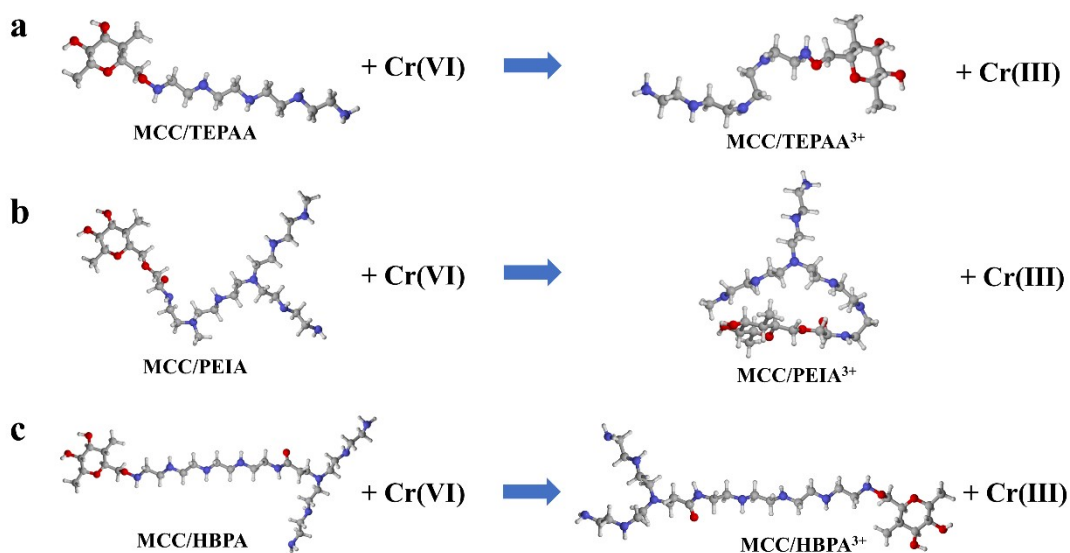


Fig. 18 Computational models of the three adsorbents and Cr cations obtained by DFT calculations: (a) MCC/TEPAA; (b) MCC/PEIA; (c) MCC/HBPA. The white, gray, blue and red colors denote H, C, N and O atoms.

The computational models of the MCC/TEPAA, MCC/PEIA, and MCC/HBPA adsorbents and Cr cations obtained by DFT calculations conducted at a temperature of 298 K and atmospheric pressure are presented in Fig. S18a–c, respectively. The Gibbs free energy values (G) related to the reactions corresponding to Cr(VI) adsorption and Cr(VI) to Cr(III) reduction processes are listed in Table S6. We note that the changes in G (ΔG) associated with these reactions were all less than zero, indicating that all processes occur spontaneously, and the preferential order for reduction rate based on increasingly negative ΔG values is MCC/TEPAA > MCC-PEIA > MCC/HBPA. These results clearly support Cr(VI) to Cr(III) reduction rate results discussed above, where the

small molecule structure is at the fast rate, followed by that of the linear molecule structure, while the hyperbranched large molecule structure is at slowest rate.

A large body of literature shows that the bulk amino groups of the adsorbents are positively charged due to protonation in the acidic solution, and Cr(VI) ions are attracted by electrostatic interaction.^{4, 6} Here, the electrostatic attraction is facilitated by the lone pairs of electrons provided by the nitrogen atoms in the amino groups, which also provide empty orbitals by chelation. Finally, Cr(VI) is reduced to Cr(III) via a redox reaction. Here, the Cr(VI) in the form of $\text{Cr}_2\text{O}_7^{2-}$ and CrO_4^{2-} in the solution is reduced to Cr(III) ($\text{Cr}(\text{OH})_3$) due to the strong oxidation of dichromate, which can easily gain electrons and will be reduced along with the decrease of the valence.⁷⁻⁹ At the same time, the protonated amino groups and unreacted N atoms on the cellulose-based solid amine adsorbent are oxidized by losing electrons.^{2, 4, 6} It's clearly illustrates the important impact of amino groups density on the Cr(VI) adsorption performance of the adsorbents, which was observed to be essentially equivalent for all three adsorbents because they were deliberately designed to have an equivalent amino groups density.

4 References

1. X. Shi, W. Lu, Y. Xue, H. Zhou, F. Xue, H. He, S. Wang and S. Wang, *Chem Eng J*, 2021, **424**, 130362.
2. F. Xue, H. He, H. Zhou, Z. Quan, Z. Chen, Q. Wu, H. Zhu and S. Wang, *Chem Eng J*, 2020, 128037-128047.
3. H. He, L. Zhuang, S. Chen, H. Liua and Q. Li, *Green Chem*, 2016, **18**, 5859-5869.

4. H. Zhou, H. Zhu, F. Xue, H. He and S. Wang, *Chem Eng J*, 2020, **385**, 123879-112890.
5. X. Guo, Y. Yao, H. Zhao, C. Chi, F. Zeng, F. Qian, Z. Liu, L. Huo and Y. Lv, *Science of The Total Environment*, 2021, **788**, 147852.
6. H. Zhou, H. Zhu, X. Shi, L. Wang, H. He and S. Wang, *Chem Eng J*, 2021, **412**, 128670-128680.
7. C. Zhu, Q. Wang, X. Huang, T. Li and G. Yang, *J Hazard Mater*, 2021, **414**, 125485.
8. H. Wang, J. Zhang, J. Zhu, J. Chang, N. Wang and H. Chen, *J Hazard Mater*, 2021, **409**, 124529.
9. Y. Sun, X. Liu, X. Lv, T. Wang and B. Xue, *Journal of Cleaner Production*, 2021, **295**, 126406.